River Flow 2010 - Dittrich, Koll, Aberle & Geisenhainer (eds) - © 2010 Bundesanstalt für Wasserbau ISBN 978-3-939230-00-7

On the impulse criterion for entrainment of coarse grains in air

M. Valyrakis & P. Diplas
Department of Civil and Environmental Engineering, Virginia Tech, Blacksburg, VA, USA
C. L. Dancey
Department of Mechanical Engineering, Virginia Tech, Blacksburg, VA, USA

ABSTRACT: The dynamic interaction between the fluctuating hydrodynamic forces and the solid particles forming the erodible boundary comprises one of the fundamental problems in fluvial hydraulics. Conventional bedload transport models, based on temporally and spatially mean quantities, fail to account for the nonlinearities inherent in the process, due to high variability of both turbulent forces and local geometrical arrangements. Recently impulse has been proposed as a potential criterion for grain entrainment. The validity of this criterion is investigated first by a series of physical experiments employing an electromagnet setup. Then a discrete particle code is utilized to reproduce the dynamics of flow-grain interplay more accurately, for entrainment levels beyond critical. The trajectories of individual spherical particles in air are numerically simulated, by considering the forces acting on the grain and solving Newton's equations of motion. It is shown that both the magnitude as well as the duration of forces (forcing history) is important in determining the overall particle response. A wide range of grain motions, from incomplete to energetic entrainments, is investigated. The results are expressed in terms of the impulse criterion demonstrating its applicability to variable degrees of particle mobility (below, at and above the threshold for complete entrainment).

Keywords: Impulsive forcing, Discrete Particle Models, Particle dislodgement

1 INTRODUCTION

Transport of sedimentary particles by water, air and ice constitutes a major problem in engineering and earth surface dynamics. Traditionally, inception of motion of grains has been studied theoretically following a static force or moments balance approach (Buffington & Montgomery 1997). Several researchers have employed numerical codes to simulate transport of bed surface material (McEwan & Held 2001, Schmeeckle & Nelson 2003). Even though they adopted a dynamical perspective, the numerical models failed to shed light to the complex interplay of flow and solids.

Recently, Diplas et al. (2008), proposed impulse (I_i), as the relevant criterion for grain entrainment. In addition, to the widely recognized role of the magnitude of the instantaneous shear stress tensor, $F(t)$ (Nelson et al. 1995, Sumer et al. 2003, Schmeeckle et al. 2007), the duration, T_i, over which it remains sufficiently high (above a critical level, F_{cr}) is of importance:

$$I_i = \int_{t_i}^{t_i+T_i} F(t)dt, \text{ for } F(t) > F_{cr} \quad (1)$$

The special case of entrainment of coarse grains in air, due to the action of impulsive forces, is investigated. Usually experiments in air are performed in wind tunnels (Bagnold 1941, Fletcher 1976, Greeley & Iversen 1985, Iversen & Rasmussen 1999), mainly examining the motion of saltating sand particles initiated by flow pressure. However, the entrainment of larger sized particles has not been adequately explored, despite the fact that it may account for up to 25% of the aeolian transport (Bagnold 1941). The entrainment of such grains termed surface creep may occur as the result of impacts with saltating particles or extreme wind bursts and its study finds application to soil erosion control and crop technology.

Here the initiation of mobilization and entrainment of coarse grains by rolling is developed theoretically based on the impulse criterion. This criterion is validated with a series of appropriately

designed bench top experiments. The theory is then compared to numerical simulations, to extend the results to variable degrees of grain mobility.

2 THEORETICAL FORMULATION

2.1 *Incipient motion for a rolling grain*

Traditionally incipient motion has been treated from a static viewpoint, utilizing force or momentum balance equations. According to the polar coordinate system (θ, ξ) shown in Figure 1, initiation of motion of an exposed spherical particle, while retaining contact with the grains comprising the solid bed, occurs for:

$$\Sigma F_\theta = F_D \sin(\theta_0) - W \cos\theta_0 > 0 \quad (2a)$$

$$\Sigma F_\xi = -F_D \cos(\theta_0) - W \sin\theta_0 < 0 \quad (2b)$$

where all forces other than the gravitational and drag are neglected, θ_0, is the pivoting angle, formed between the horizontal and the lever arm (L_{arm}), W, is the grain's weight, ΣF_ξ , ΣF_θ represent the sum of forces in the radial, ξ, and tangential, θ, directions at the rest position, respectively.

For the dynamic formulation the temporal dimension has to be accounted for. Utilizing the equations of motion for a grain rolling out of its resting pocket, Valyrakis et al. (in press) formulated the general equations of force-duration combination required for its complete dislodgement downstream. Considering the application of an impulsively applied drag, zero bed slope and air flow or negligible ratio of fluid to solid density the solution to the equation describing the particles motion in the tangential direction is simplified to:

$$T = \sqrt{\frac{L_{arm} m_{\mathrm{mod}}}{-\Sigma F_\xi}}\, arc\sinh\left(\sqrt{2W\rho_\theta}\,\frac{\sqrt{-\Sigma F_\xi}}{\Sigma F_\theta}\right) \quad (3)$$

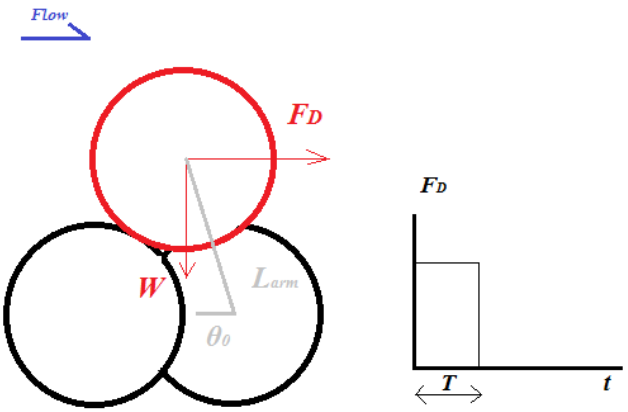

Figure 1. . Definition sketchof tetrahedral particle arrangement for entrainment by rolling, due to application of drag (F_D) force of certain duration (T, as shown in the inset).

where ρ_θ, is a geometrical coefficient depending on the ratio of exposed to base solid grains:

$$\rho_\theta = (1-\sin\theta_0)\left(\frac{\cos\theta_0}{1-\sin\theta_0}\right) \quad (4)$$

2.2 *Extension for various mobility levels*

Equation (3) describes the critical forcing conditions required to impart enough momentum for the complete dislodgement of particle downstream. A wide range of motions below critical, can actually be described, if the effect of a mobility parameter, λ, is incorporated:

$$T = \sqrt{\frac{L_{arm} m_{\mathrm{mod}}}{-\Sigma F_\xi}}\, arc\sinh\left(\sqrt{2W\rho_\theta\lambda}\,\frac{\sqrt{-\Sigma F_\xi}}{\Sigma F_\theta}\right) \quad (5)$$

where λ, is defined as the ratio of partial angular dislodgement to the angular displacement for complete entrainment:

$$\lambda = \frac{\sin(\theta_{fin}) - \sin(\theta_0)}{\sin(\frac{\pi}{2}) - \sin(\theta_0)} \quad (6)$$

Thus for a sub-critical entrainment level defined by Equation (6), the duration of applied force is predicted by the modified equation for rolling,, Eq. (5).

In the following sections, the theoretical results are validated through a series of physical experiments for sub-critical and near critical entrainment levels. A numerical code is utilized to reproduce the theoretical results for the above cases as well as extend the results to more energetic entrainment levels.

3 ELECTROMAGNET EXPERIMENTS

3.1 *Experimental setup*

The relevance of impulse to particle mobilization is demonstrated via a set of experiments. The setup (Figure 2), included a tetrahedral arrangement of spheres. The base of the arrangement consists of Teflon® spheres glued to a fixed horizontal surface. A steel spherical particle of the same diameter with the base particles (d_1=d_2=8mm), is placed on top of them. Drag forces of certain duration (T_e) and magnitude (F_e) are applied on the steel particle via an electromagnet.

The setup also included a data acquisition board (DAQ), a signal processor and a circuit used for voltage amplification. Appropriate software was used on a personal computer (PC), to generate user defined series of electromagnetic pulses of

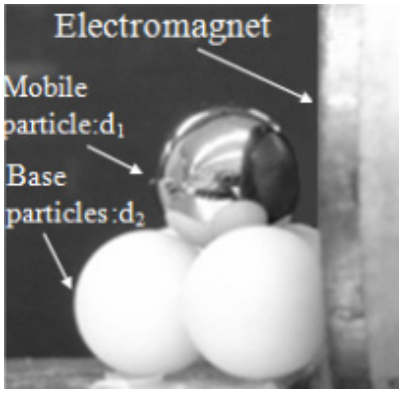

Figure 2. Experimental setup (showing grain arrangement and face of electromagnet).

varying duration and magnitude. The circuit amplifies the signal sent by the DAQ system to the magnet, reads the voltage drop across the electromagnet as well as the current and then deamplifies these signals to an appropriate range to be read back in by the DAQ.

A high speed camera was used to accurately monitor the displacement of the steel particle in still air. Observation of those videos confirmed that rolling is the mode of entrainment.

Here the impulsively generated electromagnetic field models the forces the grain experiences due to wind flow but in a controlled manner employing appropriate software and circuitry. The magnitude of electromagnetic force is proportional to the square of the voltage, V, across the electromagnet, $F_e=cV^2$, with c, a constant depending on the electromagnet specifications and the distance from the electromagnet. Consecutively, controlling the voltage and duration, a variety of electromagnetic pulses may be applied.

For a wide range of F_e, T_e combinations the response of the particle is monitored. Initially for constant voltage levels above a minimum, the duration of the electromagnetic pulse is increased (Figure 3). The gradual increase in duration is interrupted when the particle has been entirely dislodged towards the electromagnet's face. Then

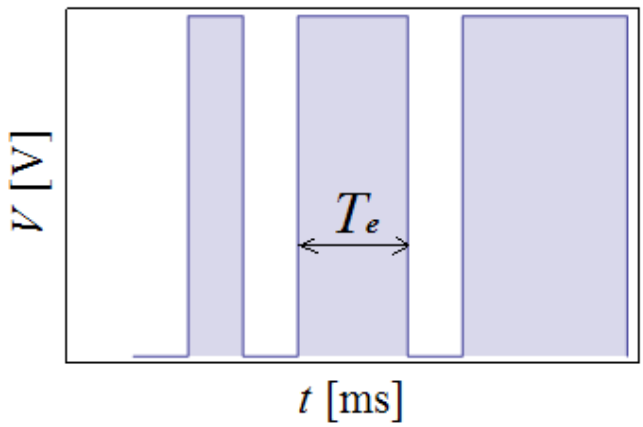

Figure 3. Representation of the generated electromagnetic pulses by changing the duration for fixed magnitude of applied electromagnetic force.

different voltages are checked for, following the same process. In this manner, information is obtained regarding the applied impulse (characteristic voltage and duration) and consequent maximum angular displacement of the sphere. The applied voltages ranged from 2.5 to 15 Volts, with a minimum voltage step size of 0.25 Volts, while the duration of their application varied from 3 to 75 ms with a time step of 2-4 ms. It should be noted that the time between the generation of the electromagnet pulses is fixed to a time greater than the required relaxation time to smooth out any grain motion due to the previously applied pulse.

Figure 4, is typical of the results of the followed procedure. In this figure, (T_e, V_e^2) data pairs are shown. Each experiment was performed up to three times to ensure repeatability and accuracy. After a wide range of T_e-F_e combinations were explored, the threshold curve indicative of the necessary and sufficient impulsive force characteristics for complete grain dislodgment, should lie between the points signifying "movement" ($\lambda \geq 1$) and those just "prior to movement" ($0.5<\lambda<1$).

A significant number of data points were collected, as shown in Figure 4. Observing the motion of the grain from the synchronized high speed camera videos, the maximum angular displacement for the applied impulses is obtained. Then the mobility ratio, λ, is computed for each of them to allow their classification from below to above threshold levels. Several mobility levels as predicted from Eq. (5) are shown on Figure 4. These curves divide the experimentally observed data points, to regions of different degrees of angular dislodgement (λ). The theoretical results (predicted, Figure 4) are in good agreement with the experimental points (observed, Figure 4), implying that for both incomplete and full grain displacement, the required force magnitude varies almost inversely with the duration.

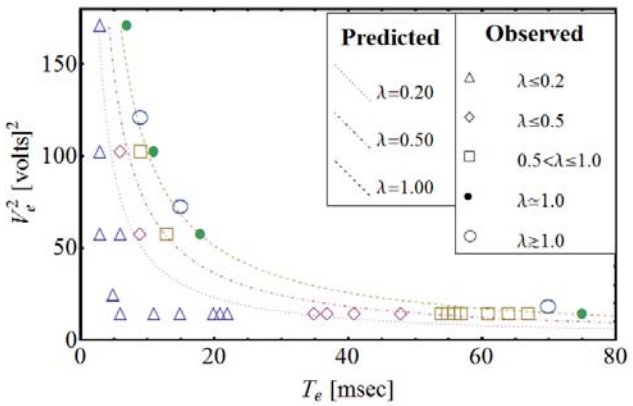

Figure 4. Comparison of different mobility levels as predicted by the theory for various values of λ (predicted), with experimentally obtained data points for changing impulse levels (observed) below, at and above critical.

3.2 *Trajectory analysis*

Using the video recorded via the high speed digital camera a detailed analysis of the motion of the mobile sphere can be performed. The camera (Phantom v. 4.2) has the ability to run at 2,100 pps at full resolution (512x512), up to 30,000 for lower resolutions. Appropriate image analysis software (Phantom 6.0.4), can be used to track selected points on the sequence of recorded frames, corresponding to the center of particle's mass. The accuracy of the analysis depends on the choice of resolution (at the cost of frame rate acquisition) and the accuracy of manual selection of points.

In this manner the software extracts the change of coordinates (x, y) of the center of the sphere, in time. A typical trajectory as observed for the case of near threshold of motion ($\lambda \geq 1$, T=15ms) is shown in Figure 5. Considering the known duration of impulse, the differential form of equation of motion of the sphere is numerically solved with a sufficiently small time step, to obtain the magnitude of force that predicts a trajectory, as best fit to the observed one (Figure 5). Following the same process for a number of data points near the critical conditions ($\lambda \geq 1$), the constant c, can be predicted (Figure 6).

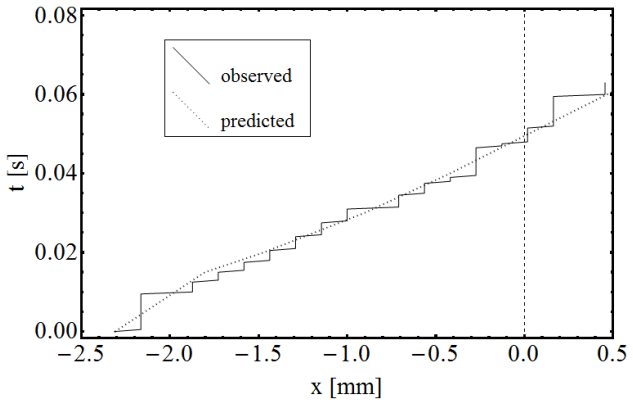

Figure 5. Characteristic particle trajectory (for T=15ms) obtained from tracking its center of mass with the high speed camera (observed) and best fit curve to the trajectory obtained from the numerical solution of equation of motion (predicted).

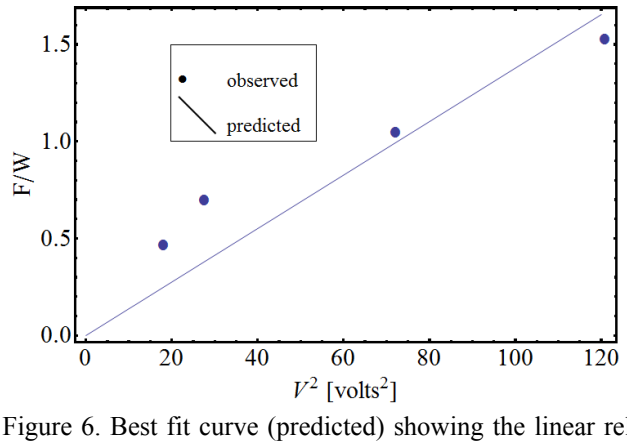

Figure 6. Best fit curve (predicted) showing the linear relation of electromagnetic force to the square of voltage and corresponding experimental data points (observed).

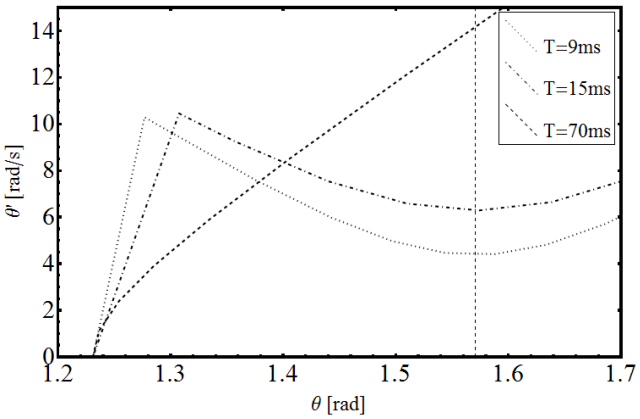

Figure 7. Characteristic particle trajectories for near critical level ($\lambda \geq 1$), as predicted from the numerical solution of equation of motion (to match the observed trajectories).

For the case of insufficient impulse durations the particle will perform incomplete movements observed to twitch and then fall back to its pocket ($\theta=\theta_0$) under the influence of gravity, before reaching the topmost position ($\theta=\pi/2$, dotted vertical line, Figure 7).

For the case of near and above critical level typical grain trajectories are represented in phase-space diagrams (Figure 7), plotting the angular displacement, θ, versus the momentum represented by the angular velocity, θ'.

The dynamics of the grain dislodgement, for the various cases of impulse duration, are clearly demonstrated. An accelerating phase is initially seen due to the action of the applied force. The impulse is proportional to the change of particle's momentum, so this plot also provides information on the magnitude of offered impulses. For low durations relative to the time for complete particle displacement out of its pocket (e.g. T=9 and 15 ms), a decelerating phase due to the resisting gravitational force is discerned. However, if the impulse duration (e.g. T=70 ms), is longer than the dislodgement time, the sphere will continuously accelerate.

3.3 *Impulse representation of results*

In agreement with the results of the theoretical analysis, while the range of electromagnetic force (F_e parameterized by V^2), changes over an order of magnitude (e.g. from 13 to 175 volts^2, Figure 7), the impulse computed as the product $I_e = F_e T_e$, remains almost invariable over the range of tested durations (e.g. the change of theoretically predicted I_e is less than 6%), for impulses corresponding to particular grain movements.

The angular velocity, θ', at the topmost position ($\theta=\pi/2$), is an indicator for the kinetic energy of the sphere, E_{kin}. Critical entrainment by definition corresponds to $E_{kin}=0$ at $\theta=\pi/2$. The greater the kinetic energy of the particle is at this position,

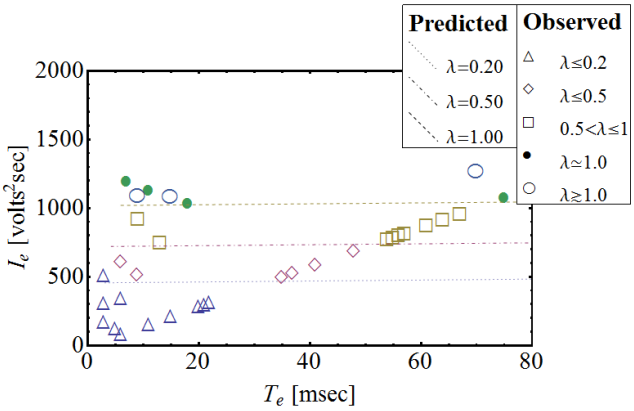

Figure 7. Required impulse levels for various degrees of grain mobilization as predicted from the theory (predicted) or obtained from the electromagnet experiments (observed).

the higher the momentum initially imparted as well as the offered impulse. This observation is confirmed more clearly if the results are offered in terms of impulse (Figure 7). As expected, the highest energy levels correspond to the greatest impulses offered (e.g. T=70 ms).

4 NUMERICAL SIMULATIONS

4.1 *Discrete particle method*

There is an increased interest of hydraulic researchers studying the dynamics of sediment transport in employing numerical methods such as the discrete particle modeling (DPM) technique (Drake & Calantoni 2001, McEwan & Heald 2001, Calantoni et al. 2004, McEwan et al. 2004, Valyrakis et al. 2008, Yeganeh-Bakhtiary et al. 2009). Here, this numerical tool is used to predict the grain response for different impulse levels to validate the theoretical results for the cases of sub-critical and critical entrainment. The results are also extended for the case of super-critical entrainments.

A commercial DPM algorithm, Particle Flow Code in three dimensions (PFC3D), is employed to model the behavior of the impulsively loaded exposed sphere. PFC3D is a computational program which models the dynamics of systems of particles by numerically integrating the fully coupled equations of motion (Itasca 2003). For the numerical solution, explicit finite difference schemes are employed.

The grains are modeled as spherical particles, even though different shapes are possible by clumping particles of different sizes together. In general, PFC3D is a micro-mechanical code, meaning that the macroscopic behavior of the granular system is defined by the microscopic properties of the individual particles, typically requiring a calibration process (Chen et al. 2007, Tawadrous et al. 2009). The properties of grains composing the bed are chosen to correspond to realistic physical conditions (Table 1). Variations from these parameters did not appear to affect the outcome of the simulations.

Table 1. General setup and particle properties used for the numerical simulations (PFC3D)

Normal and shear stiffness (N/m)	10^8
Friction coefficient	0.5
Maximum time step	10^{-4}
Local damping factor	0.0
Normal and shear viscous damping coefficient	0.5
Gravitational acceleration (m/s^2)	9.81

The time step is important in the calculation process, since if it is very large it may lead to numerical instability, while if very small the duration of simulation will be significantly extended. The chosen time step ensures both numerical stability as well as adequate precision for the numerical runs.

General viscous damping (Bishop & Johnson 1960) is implemented, so that the damping force opposes the grain movement with magnitude proportional to its velocity. The proportionality constant (Ginsberg & Genin 1984) is defined through the viscous damping coefficient (Table 1), the equivalent mass of the particles in contact and the contact stiffness.

Frictional or shear contact forces are traditionally computed based on the normal force and the friction coefficient (Table 1). If its maximum value is greater than the applied shear force then slip may occur.

4.2 *Description of numerical procedure*

Initially the geometry of the particle assembly is provided. A horizontal layer of closely packed spheres is fixed in space, on a hexagonal arrangement (Figure 8). A mobile sphere is positioned at a predefined location on top of three bed particles, so that it forms a tetrahedral micro-topography. The downstream and lateral dimensions of the bed layer are significantly greater than the expected

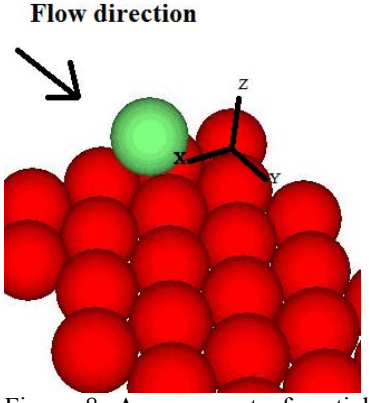

Figure 8. Arrangement of particles (bed configuration and mobile grain), employed for the numerical simulations.

maximum grain dislodgement expected for the variable impulse levels investigated herein. All grains share the same material properties, are homogeneous and of the same size.

The mobile sphere is loaded impulsively with a horizontal force of varying duration, until the target response is obtained. Three characteristic mobility levels are examined referring to the subcritical, critical and supercritical entrainment.

4.3 *Comparison of theory with numerical simulations*

The results of the simulations are shown in Figure 9, appropriately normalized to allow for their general interpretation. The applied force is normalized by grain's weight ($F_{norm}=F/W$) and the duration with the required time for the grain to perform a free fall for a vertical distance equal to its diameter.

Normalizing in a similar manner Equation (5), the theoretically predicted curves providing a best fit to the observed numerical data are given. It is seen that the numerical runs provide an almost perfectly match.

Even though the mobility parameter, λ (Eq. 6), is mathematically limited to values below unity, implementation of values higher than one are shown to adequately predict supercritical grain entrainment levels. In Figure 9, a direct comparison of theory and simulations is shown. For subcritical case of λ=0.27, the grain is displaced to a maximum angular displacement of 6/22 of its maximum potential energy. The critical case (λ=1), indicates the minimum impulse level required to move the grain only one pocket downstream. The minimum impulse for supercritical or energetic entrainment of three pockets downstream corresponds to λ=3.7.

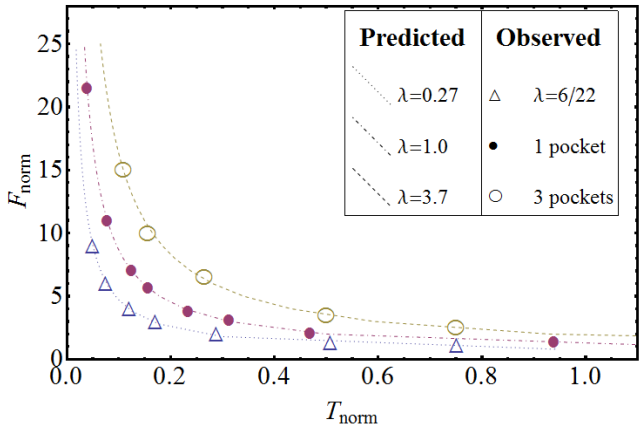

Figure 9. Comparison of the force-duration combinations required to produce different grain response from the simulations (observed) with the corresponding levels as dictated from the theory (predicted).

4.4 *Impulse representation of results*

Figure 10, demonstrates the variation of normalized impulse ($I_{norm}=F_{norm}T_{norm}$) with normalized duration for the different degrees of entrainment. The approximate constancy of impulse over a large range of durations seen from the physical experiments is also reproduced numerically.

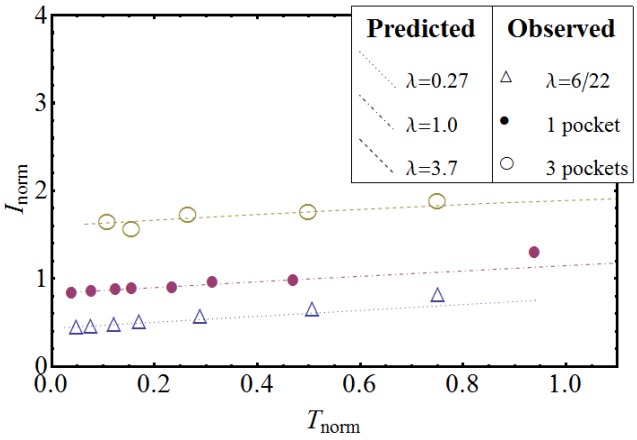

Figure 10. Representation of the required impulse levels for different degrees of grain mobilization as predicted from the theory (predicted) and from simulations (observed).

4.5 *Trajectory analysis*

Building appropriate Fish language commands, user defined functions are created to monitor the time history of a variable of interest. In particular, variables characterizing the trajectory of the grain such as its potential and kinetic are computed and recorded at each time step. The results are shown on Figure 11, normalized by the potential energy of the particle with its center of mass elevated to a height equal to its diameter.

The cases of critical (1 pocket) and supercritical (3 pockets) entrainments are demonstrated for relatively low and high durations respectively. Comparing the maximum levels of obtained kinetic energy, it is apparent that the case of entrainment of grain further downstream (3 pockets), required higher impulse levels, corresponding to greater energy.

Over the acceleration phase the particle gains kinetic energy, which is eventually stored in the form of potential energy. The longer the duration of the acceleration phase is, the greater the ratio of potential to kinetic energy will be (e.g. compare Figure 10a and b).

The energy of grains is mainly dissipated due to the aforementioned mechanism of viscous damping. This mechanism is activated when the mobile particle collides with those comprising the bed (as shown at the instances of minimum potential energy (Figure 10c and d). Regarding the case of supercritical entrainment, longer force dura-

tions will result to greater times required for the grain to travel past the first pocket.

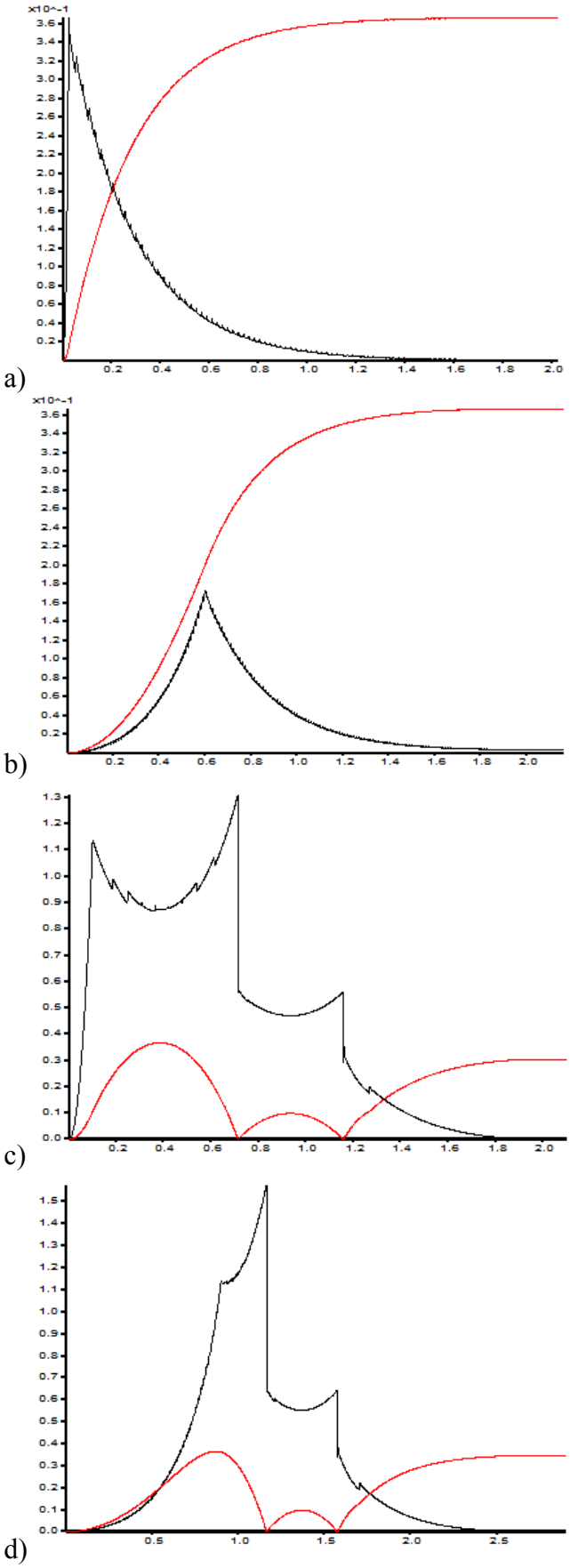

Figure 10. Potential (red) and kinetic energy for typical particle trajectories: a) low T, critical level, b) high T, critical level, c) low T, energetic dislodgement and d) high T, energetic dislodgement.

5 CONCLUSIONS

The theoretically derived impulse criterion is evaluated for the entrainment of coarse spherical particles on air. Impulse is a physically sound criterion for such cases, appropriate to model wind gusts and collision forces from entrained grains. The applications for which this criterion may be relevant are reported.

A novel experimental setup including an electromagnet is employed to validate the theory for incomplete to full sphere dislodgement. To further investigate the dynamics of grain movement a trajectory analysis is performed, utilizing a high speed camera.

The above results are additionally reproduced with numerical simulations of a commercial discrete particle method (PFC3D). The code provides the ability to further extend the results to the case of supercritical degrees of entrainment. The normalized energy representation of the particle trajectories is performed. DPM have increased potential since they offer the ability to easily and effectively expand the results, by simply changing the values of certain parameters of the system.

ACKNOWLEDGEMENT

The support of the National Science Foundation (EAR-0439663 and EAR-0738759) is gratefully acknowledged.

REFERENCES

Bagnold, R. A. 1941. The Physics of Blown Sand and Desert Dunes. London, Chapman and Hall.

Bishop, R. E. D., Johnson, D. C. 1960. The mechanics of vibration. Cambridge University Press, Cambridge, U.K.

Buffington, J. M., Montgomery, D. R. 1997. A systematic analysis of eight decades of incipient motion studies, with special reference to gravel-bedded rivers. Water Resources Research, 33(8), 1993-2029.

Calantoni J., Holland K. T., T. G. Drake. 2004. Modelling Sheet-Flow Sediment Transport in Wave-Bottom Boundary Layers Using Discrete-Element Modelling. Philoshophical Transactions Royal Society of London, Series A-Math. Phys. Eng. Sci., 362(1822), 1987-2001.

Chen, F., E. C. Drumm, G. Georges 2007. Prediction/Verification of Particle Motion in One Dimension with the Discrete-Element Method. International Journal of Geomechanics, 7(5), 344-352.

Church, M., Hassan, M. A., Wolcott, J. F. 1998. Stabilizing self-organized structures in gravel-bed stream channels: Field and experimental observations. Water Resourses Research, 31(11), 3169-3179.

Diplas, P., Dancey, C. L., Celik, A. O., Valyrakis, M., Greer, K., Akar, T. 2008. The role of impulse on the initiation of particle movement under turbulent flow conditions. Science, 322, 717-720

Diplas, P., C. L. Dancey, Valyrakis M., A. O. Celik. 2009. The role of Turbulence on the initiation of sediment movement. Powders and Grains 2009, Proceedings of the 6th International conference on micromechanics of granular media, Golden, Colorado, 13-17 July 2009.

Drake, T. G., Calantoni, J. 2001. Discrete particle model for sheet flow sediment transport in the nearshore. Journal of Geophysical Research, 106(C9), 19,859-19,868.

Fletcher, B. 1976. The incipient motion of granular materials. Journal of Physics D: Applied Physics 9(17), 2471-2478.

Greeley, R., Iversen, J. D. 1985. Wind as a Geological Process. Cambridge UK, Cambridge University Press.

Ginsberg, J. H., Genin, J. 1984. Statics and dynamics, Wiley, Hoboken, N.J.

Iversen, J. D., Rasmussen, K. R. 1999. The effect of wind speed and bed slope on sand transport. Sedimentology 46(4), 723-731.

Itasca. 2003. Particle Flow Code, PFC3D, release 3.0. Itasca Consulting Group, Inc., Minneapolis, Minnesota.

McEwan I., Heald J. 2001. Discrete particle modeling of entrainment from flat uniformly sized sediment beds. Journal of Hydraulic Engineering, 127(7), 588-597.

McEwan, I., Sørensen, M., Heald, J., Tait, S., Cunningham, G., Goring, D., Willetts, B. 2004. Probabilistic Modeling of Bed-Load Composition. Journal of Hydraulic Engineering, 130, 129-139.

Nelson, J. M., Shreve, R. L., McLean, S. R., Drake, T. G. 1995. Role of near bed turbulence structure in bed load transport and bed form mechanics. Water resourses research, 31(8), 2071-2086.

Nikora V. I., Heald, J., Goring D., McEwan I. 2001. Diffusion of saltating particles in unidirectional water flow over a rough granular bed. Journal of Physics A, 34, L743–L749.

Paintal, A. S. 1971. A stochastic model of bed load transport. Journal of Hydraulic Research, 9(4), 527–554.

Papanicolaou A. N., Diplas, P., Evaggelopoulos N., Fotopoulos S. 2002. Stochastic Incipient Motion Criterion for Spheres under Various Bed Packing Conditions. Journal of Hydraulic Engineering, 128(4), 369-380.

Papanicolaou A. N., Schuyler A. 2003. Cluster Evolution and Flow-Frictional Characteristics under Different Sediment Availabilities and Specific Gravity. Journal of Engineering Mechanics, 129(10), 1206-1219.

Reid, I., Frostick, L. E., Brayshaw, A. C. 1992. Microform roughness elements and the selective entrainment and entrapment of particles in gravelbed rivers. Dynamics of Gravel-bed Rivers, John Wiley and Sons Ltd., 253-275.

Schmeeckle M. W., Nelson J. M. 2003. Direct numerical simulation of bedload transport using a local, dynamic boundary condition. Sedimentology, 50(2), 279-301.

Schmeeckle M. W., Nelson J. M., Shreve R. L. 2007. Forces on Stationary Particles in Near-Bed Turbulent Flows. Journal of Geophysical Research, 112, F02003.

Singh, K. M., Sandham, N. D., Williams, J. J. R. 2007. Numerical Simulation of Flow over a Rough Bed. Journal of Hydraulic Engineering, 133(4), 386-398.

Smith, C. R., 1996. Coherent flow structures in smooth-wall turbulent boundary layers: Facts, mechanism and speculation, in Coherent Flow Structures in Open Channels. P. J. Ashworth et al. (ed.), 1–39, John Wiley, New York.

Strom, K., Papanicolaou, A. N., Evangelopoulos, N., Odeh, M. 2004. Microforms in Gravel Bed Rivers: Formation, Disintegration, and Effects on Bedload Transport. Journal of Hydraulic Engineering, 130, 554.

Tawadrous, A. S., DeGagné, D., Pierce, M., Mas Ivars, D. 2009. Prediction of uniaxial compression PFC3D model micro-properties using artificial neural networks. International Journal for Numerical and Analytical Methods in Geomechanics, 33(18), 1953-1962.

Yeganeh-Bakhtiary, A., Shabani, B., Gotoh, H. 2009. A three dimensional distinct element model for bed-load transport. Journal of Hydraulic Research, 47(2), 203-212.

Valyrakis M., Diplas P., Celik A. O., Dancey C. L. 2008. Investigation of evolution of gravel river bed microforms using a simplified Discrete Particle Model, Proceedings of River Flow 2008, Ismir, Turkey, 03-05 September 2008, 10p.